Available online at www.sciencedirect.com
SCIENCE DIRECT®
International Journal of Thermal Sciences 43 (2004) 185–200
International Journal of Thermal Sciences
www.elsevier.com/locate/ijts

Enhanced heat transfer of forced convective fin flow with transverse ribs

Shyy Woei Chang [a,*], Lo May Su [b], Tsun Lirng Yang [c], Shyr Fuu Chiou [a]

[a] *Thermal Fluids Laboratory, National Kaohsiung Institute of Marine Technology, No. 142, Hai-Chuan Road, Nan-Tzu District, Kaohsiung, Post code 811, Taiwan, ROC*
[b] *Department of Electrical Engineering, Tung Fang Institute of Technology, Taiwan, ROC*
[c] *Department of Electrical Engineering, Fortune Institute of Technology, Taiwan, ROC*

Received 6 January 2003; accepted 16 June 2003

Abstract

This experimental study investigates the heat transfers in three side-opened and bottom-sealed rectangular channels with two opposite walls roughened by 90° staggered ribs, which simulate the enhanced cooling passages in the fin-type heat sinks of electronic chipsets. The various degrees of interactive effects due to the surface ribs, side-profile leakage flows and streamwise weakened coolant flow are functionally related with Reynolds number (Re) and channel length-to-gap ratio (L/B), which unravel the considerable impacts on local and spatially averaged heat transfers over the rib-roughened fin surfaces. A selection of detailed heat transfer measurements over the rib-roughened fin surfaces illustrates the manner by which the isolated and interactive influences of Re and L/B-ratio affect the local and spatially averaged heat transfers. Relative to the heat transfer results acquired from the smooth-walled test channels, the augmentations of spatially averaged heat transfers generated by the present surface ribs are in the range of 140–200% of the flat fin reference levels. In conformity with the experimentally revealed heat transfer physics, a regression-type analysis is performed to develop the correlation of spatially-averaged Nusselt number over rib-roughened fin surface, which permits the individual and interactive effect of Re and L/B on heat transfer to be evaluated. A criterion for selecting the optimal length-to-gap ratio of a fin channel, which provides the maximum convective heat flux from the rib-roughened fin surface, is formulated as an engineering tool to assist the design activity for the cooling device of electronic chipsets.

Keywords: Ribbed fin flow; Forced heat convection

1. Introduction

The ever-mounting intensified integration density of electrical circuits in an electronic chipset constantly necessitates the heat transfer augmentation for its heat sink, which widely adopts the pin-fin arrays. As an illustrative example, the thermal power of an Intel CPU with an area for heat dissipation of about 10 mm × 10 mm is increased to the range of 30–80 W from 10–15 W. This increased power consumption provides the heat flux of 300–800 kW·m^{-2} over a CPU unit which requires the effective cooling scheme to maintain the operating temperature at about 80 °C [1]. To cope with the increasing cooling required for an electronic chipset, a variety of cooling schemes, such as the electroosmotic driven microflow, the heat pipe, the impingement jet-array and the microchannel cooling [2–5] have been developed which are suitable for installation in the electronic devices. Among these various cooling schemes, where the coolant stream impinges onto pin-fin arrays under which the powered chipset is attached, there have been considerable heat transfer augmentations demonstrated [6–15]. As illustrated in Fig. 1 for the fan-fin type cooling-scheme, the coolant stream facilitated by a cooling fan is directed into a fin-array. The extended surfaces of fin assembly provide fin effect to improve the overall heat transmission. There are several openings across a longitudinal fin to provide additional flow paths for the spent flow to convect heat out of the confined fin-channels in order to avoid the development of stagnant hot plume among the central region of the fin assembly. The internal coolant stream confined in any pair of longitudinal fins is therefore subject to continuous leakages from two side openings prior to impinging on the bottom surface of each channel. As a result, the streamwise convective capability over a fin surface is continuously undermined from the fan exit toward the bottom sealed end. Although the increase of fin-length increases the extended surface for heat transfer,

* Corresponding author.
E-mail address: swchang@mail.nkimt.edu.tw (S.W. Chang).

1290-0729/$ – see front matter
doi:10.1016/j.ijthermalsci.2003.06.006

Nomenclature

English symbols

A, C, D, n	correlative coefficients	
a	smooth entry length of rib-roughened surface	m
B	gap of test channel	m
d	hydraulic diameter of test channel	m
e	rib height	m
k_f	thermal conductivity of coolant	$W{\cdot}m^{-1}{\cdot}K^{-1}$
L	length of test channel	m
l	rib land	m
$\dot{m}$	coolant mass flow rate	$kg{\cdot}s^{-1}$
Nu	local Nusselt number over rib-roughened fin surface $= \frac{qd}{k_f(T_w - T_f)}$	
$\overline{Nu}$	spatially averaged Nusselt number over rib-roughened fin surface	
Nu_{SW}	local Nusselt number over smooth-walled fin surface	
$\overline{Nu}_{SW}$	spatially averaged Nusselt number over smooth-walled fin surface	
P	rib pitch	m
q	convective heat flux	$W{\cdot}m^{-2}$
Re	Reynolds number $= \frac{2\dot{m}}{\mu(B+W)}$	
T_w	wall temperature at fin surface	K
T_f	reference fluid temperature	K
W	width of test channel	m
x, y	coordinates in streamwise and spanwise directions	m

Greek symbols

μ	dynamic viscosity of coolant	$kg{\cdot}s^{-1}{\cdot}m^{-1}$

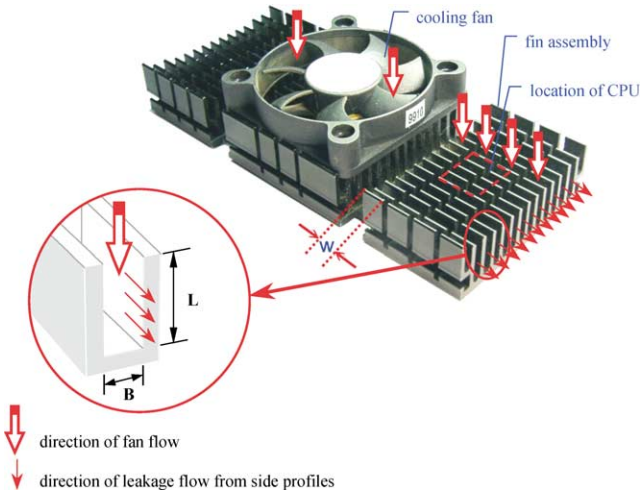

Fig. 1. Cooling configuration of forced convective fan-fin flow.

the accompanied coolant leakages from the side openings increase in an accumulative manner so that the convective capabilities in further downstream locations are accordingly weakened. Therefore the optimal selection of fin-length to fin-gap ratio should embody both considerations for the increased cooling area and its consequential effects on the heat transfer impediment due to the side-profile leakages.

When each cooling passage in the fin assembly is treated as a side-opened channel with the bottom end sealed, as shown in Fig. 1, the surface enhancement method of fitting various types of repeated ribs on a fin surface can be applied to enhance the forced convection over the fin surface. Based on the results revealed from rib-roughened duct flows, the effectiveness of surface ribs on heat transfer augmentation varies with the geometrical features of ribs such as the rib-arrangement, rib height, rib pitch, angle of attack, rib orientation and rib shape [16–19]. The overall rib-effects on heat transfer in a fully confined duct are improved heat transmission and modified spatial heat transfer distributions. Although the use of surface ribs has been the subject of much fundamental research over the years, the detailed heat transfer measurements over a rib-roughened surface in a channel with two side openings and a sealed bottom end are not available in the open literature. No previous research effort performs heat transfer measurements over a rib-roughened fin surface to explore the interactive impacts of side-profile leakage flow, rib-associated flow phenomena and streamwise weakened coolant mass flux on heat transfer. To this end, several key factors related to the design of rib-enhanced air-cooled electronic packages, such as the optimization of fin spacing and gaps between extended fins arrays and the criteria available for a designer to define the geometries of fins heat sinks, need to be unraveled [13]. This lack of fundamental knowledge and a database available for such rib-roughened flow system has been the motivation for the present study. Heat transfer measurements over the rib-roughened fin surfaces of a simulating coolant channel with the bottom-end sealed and two side-profiles opened to ambient are performed. The detailed distributions of local Nusselt number contours and the spatially averaged heat transfer data, evaluated from the infrared thermal images of the rib-roughened fin surfaces, are presented over a range of Reynolds numbers for channels with three different height-to-gap ratios. All the test channels have identical values of channel width and gap, and therefore the same hydraulic diameter. The impacts of channel height-to-gap ratio and Reynolds number on the convective heat transfer over the rib-roughened fin surface for such open boundary channel flows are subsequently analyzed. This assists the derivation of physically consistent empirical heat transfer correlations. A criterion for optimal selection of channel height-to-gap ratio that maximizes the convective capability of a rib-roughened fin surface is developed to assist the design

of fan-fin heat sinks for cooling application of electronic packages.

2. Experimental details

For a given coolant mass flow rate fed into each channel confined by a pair of longitudinal fins as typified in Fig. 1, the streamwise variation of side-profile leakage flow, and thus the spatial distribution of coolant mass flux, are functionally related with the surface condition of fin, the geometries of test channel and the thermal boundary condition imposed. The forced convection taking place within such channel could be specified by defining the total mass flux of coolant fed into the channel for a particular set of geometrical and thermal boundary conditions simulated by a heat transfer test module. Therefore the Reynolds number evaluated from the total coolant mass flux fed into the opened fin-channel is treated as the controlling flow parameter that dominates the heat transfer characteristics when the Prandtl number of coolant remains constant. In view of the geometrical conditions, the opened fin-channel is specified by the cross sectional shape, the width-to-gap ratio and the surface condition of the test channel. When the surface condition and the width-to-gap ratio of an opened fin-channel remain invariant, the length-to-gap ratio becomes the controlling geometrical parameter. The present experimental study adopts the parametric approach to characterize the heat transfer of opened fin channel flow using *Re* and L/B ratio as the controlling dimensionless flow and geometric parameters. The isolated and interactive *Re* and L/B ratio effects on heat transfer are examined.

2.1. Apparatus

The experimental apparatus is shown in Fig. 2. The test fluid, pressurized air, was directed via a flow calming section (1) with equivalent straight length of 150 mm into a settling chamber of dimensions 250 mm × 100 mm × 8 mm (2), and directed into the heat transfer test section (3). Four 10 mm thick Teflon plates constitute the settling chamber. The back surface of settling chamber (2) was extended to form the insulating wall of heat transfer test section (3). A K-type thermocouple penetrated into the settling chamber (2) to measure the coolant entry temperature, T_f, which measurement was treated as the fluid reference temperature to define the convective heat transfer coefficient and the fluid properties. These include the specific heat, thermal conductivity and viscosity of coolant, for the evaluations of Reynolds, Prandtl and Nusselt numbers. The two opposite heated surfaces, simulating a pair of fins, are made from a continuous, very thin (0.1 mm) and 100 mm wide stainless steel-foil (4). This heating foil (4) was folded to shape the inner profiles of smooth-walled and rib-roughened heat transfer test sections (3). For each surface condition, three sets of heating foil were manufactured to construct three heat transfer test sections (3) with channel lengths of 170.5, 108.5 and 47.1 mm. The generation of heat transfer data from the smooth-walled heat transfer test channels is treated as the references to assess the heat transfer enhancement provided by the present rib geometry.

The bottom sealed-end was made of a 10 × 100 × 8 mm Teflon plate (5) that provided the thermal insulation for the bottom heated surface. Two copper bars that connect the electrical terminals with the electrically heated foil (4) were secured on the flanges of the settling chamber (2) to form a complete electrical circuit. The adjustable high-current DC electrical power was fed directly into the heating foil (4) to generate the basically uniform heat-flux heating surface. As the heating foils also covered the two opposite wide walls of flow settling chamber (2), the developments of hydraulic and thermal boundary layers proceeded almost simultaneously from the immediate entrance of settling chamber (2). It is to be noted that the width and gap of all heat transfer test sections are identical with the inner width and gap of the settling chamber (2). The hydraulic diameter of test section is thus an invariant length scale of 14.8 mm. It was intended to compare the various heat transfer performances over a range of Reynolds numbers with three different channel length-to-gap ratios based on the same amount of total coolant mass flow rate. Therefore, the length scale selected to define the dimensionless flow parameters, namely the Reynolds and Nusselt numbers, is the hydraulic diameter of test section.

As shown in Fig. 2, the repeated full transverse ribs were arranged in a staggered manner on two opposite heating surfaces. Each rib-roughened surface is produced by forging the thin stainless steel foil into the geometry specified in terms of five non-dimensional groups defined in Fig. 2 of

$$\frac{\text{smooth entry length}}{\text{channel width}}\ \text{ratio} = \frac{a}{W} = \frac{4\ \text{mm}}{100\ \text{mm}} = 0.04$$

$$\frac{\text{rib height}}{\text{channel gap}}\ \text{ratio} = \frac{e}{B} = \frac{2\ \text{mm}}{8\ \text{mm}} = 0.25$$

$$\frac{\text{rib pitch}}{\text{rib height}}\ \text{ratio} = \frac{P}{e} = \frac{20\ \text{mm}}{2\ \text{mm}} = 10$$

$$\frac{\text{rib land}}{\text{rib height}}\ \text{ratio} = \frac{l}{e} = \frac{2\ \text{mm}}{2\ \text{mm}} = 1$$

Two additional dimensionless geometric parameters defining the generic features of test channels are summarized as follows:

$$\text{Aspect ratio of cross-sectional shape of test section} = \frac{W}{B} = \frac{100\ \text{mm}}{8\ \text{mm}} = 12.5$$

$$\frac{\text{channel length}}{\text{channel gap}}\ \text{ratio} = \frac{L}{B} = 5.89,\ 13.56 \text{ and } 21.33$$

Prior to entering the flow calming section (1), the air fed from the IWATA SC 175C screw-type compressor unit was dehumidified and cooled to the ambient temperature through a refrigerating unit that was integrated with the

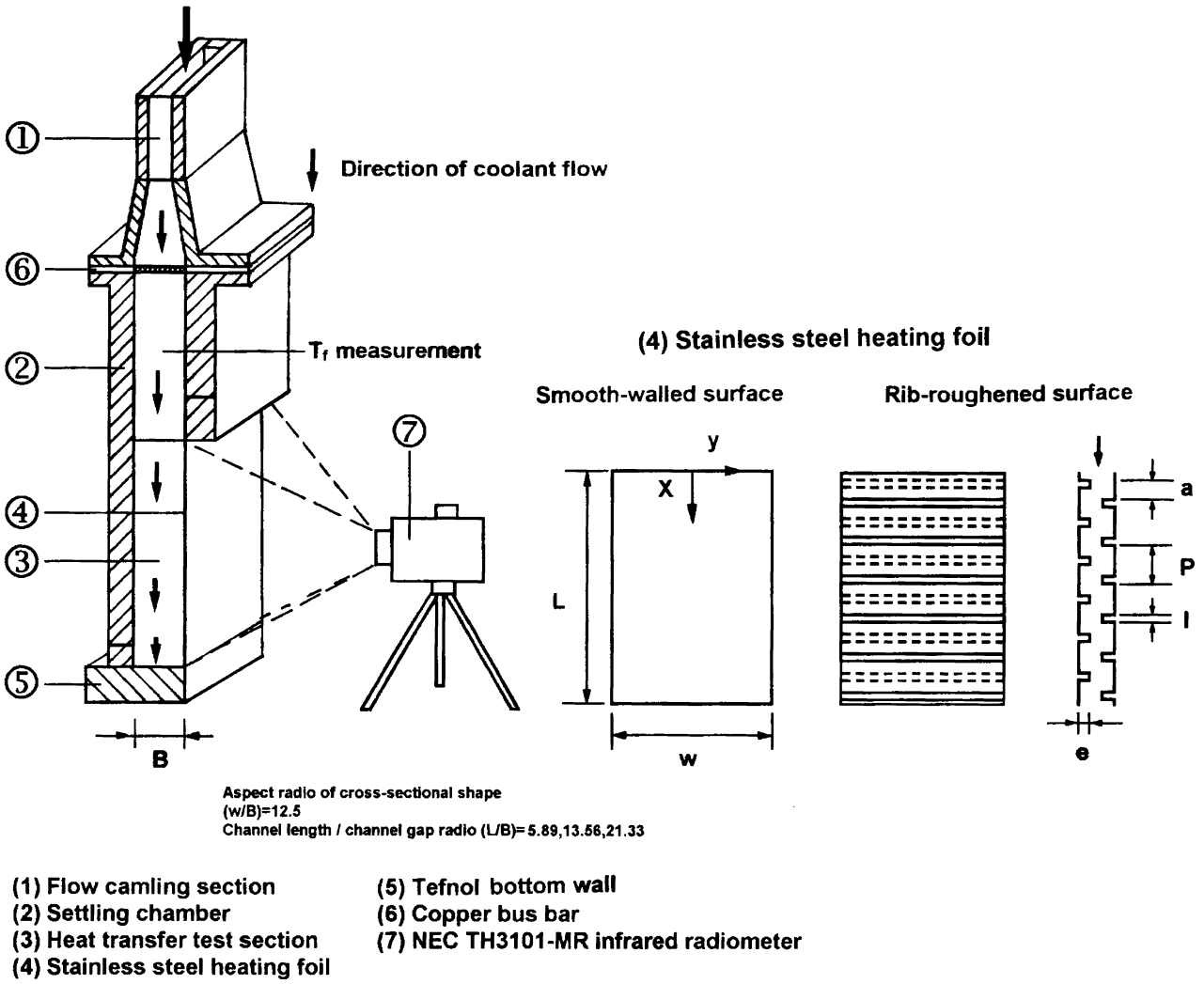

Fig. 2. Constructional details of heat transfer test module.

compressor. The dry and cooled airflow was then guided through a set of pressure regulator and filter with the mass flow rate to be metered and adjusted by a Tokyo Keiso TF-1120 mass flow meter and a needle valve, respectively. A pressure transducer connected with a digital type encoder was used to measure the pressure level of coolant flow. The complete heat transfer test unit was fixed and vertically centered on a base-frame (5). However, after several heat transfer test runs, the spatially varied thermal expansion caused by the non-uniform wall temperature fields has led to foil deflections. The maximum foil deflection measured by a precision caliper after completing the entire set of experiments was less than 0.16 mm. The temperatures of the heating surface under each test condition were imaged by a calibrated two-dimensional NEC TH3101-MR infrared radiometer (6). For this thermal image processing system, it took 0.3 seconds to complete a full-field of 239×255 matrix scan. The back surface of the heating foil (4) was painted black in order to minimize the background reflection and to increase the emission.

2.2. Program and data processing

The present experimental study involved three phases. Initially the influences of channel length-to-gap ratio and Reynolds number on heat transfer were checked out with a series of baseline tests performing at Reynolds numbers of 500, 1000, 2000, 3000 and 3300 using smooth-walled three sets of test channel with L/B ratios of 5.89, 13.56 and 21.33. The data generated in this phase revealed the characteristic thermal physics of such fan-fin flow and was treated as the reference to compare against the results acquired in the send phase of study using the rib-roughened test channels in order to unravel the heat transfer enhancements provided by the present rib geometry. The various heat transfer distributions over three rib-roughened heating surfaces with different L/B ratios for any Reynolds number tested were compared to reveal the impacts of L/B ratio on the detailed heat transfer distributions over the rib-roughened fin surface. The third phase of regression-type analysis derived the heat transfer correlation that permits the evaluation of

spatially averaged heat transfer level over the rib-roughened fin surface and developed the criterion for optimal selection of channel height-to-gap ratio from the viewpoint of maximizing the convective capability of a fin surface for air cooling of electronic packages.

The steady state heat transfer measurements were performed at each set of predefined Reynolds number and heating power. A steady state was assumed when the variations of wall temperatures with several successive scans over the heating surface were less than 0.3 °C. This generally took about 30 minutes after the adjustment of flow rate or heating power was made. Having satisfied the criterion for steady state assumption, the on-line infrared thermal-image data capture system was then activated to record and store the full field wall temperature distributions over the heating surface. Along with the measured heating power and coolant entry temperature, T_f, the local Nusselt number distributions over the heating surface at the prescribed Reynolds number and channel length-to-gap ratio were evaluated. Note, as it is attempted to compare the various heat transfer performances over the rib-roughened fin surfaces with different channel length-to-gap ratios, the Reynolds number is evaluated based on the total amount of mass flow rate fed into the test channel with the same characteristic length scale of hydraulic diameter of an opened test channel. The fluid properties required to evaluate the Reynolds number was determined from the coolant entry temperature, T_f. The various heat fluxes fed into the test section could therefore affect the Reynolds number even if the total amount of coolant mass flow rate remained invariant. Alternatively, by adjusting the coolant mass flow rate to compensate the temperature affected fluid property variations, the maximum variation in Reynolds number at the entry plane of flow settling chamber was controlled with ±1% for each individual test. The range of Reynolds numbers selected ($500 \sim 3300$) ensured that the laminar, transitional and turbulent flow conditions at the exit of flow settling chamber were examined.

The local Nusselt number, *Nu*, are evaluated using the equation of

$$Nu = \frac{qd}{k_f(T_w - T_f)} \tag{1}$$

in which the convective heat flux, q, was calculated from the electrical dissipation measured over the entire heating surface with the heat loss to be subtracted. The characteristics of external heat loss at different heating levels were determined by a number of heat loss calibration runs. For each set of calibration test runs, the flow was blocked off and the fiberglass thermal insulating material was filled in the flow passage. The heat supplied to the heating foil was therefore entirely lost into atmosphere through the conductive network of test assembly and from the back of the exposed heating surface through free convection. The supplied heating power was balanced with the external heat loss at the corresponding steady-state temperature distribution. Due to the uniformities of electrical heating power and the thermal insulation over the heating surface, the wall temperatures over the entire scanning area were distributed uniformly for heat loss calibration run. A review of the temperature data collected from the calibration test runs showed less than 3.62% of non-uniformity in the wall temperature distributions. Thus, by plotting the heat loss flux against the corresponding steady wall-to-ambient temperature, the difference revealed a linear-like functional relationship between the heat loss flux and the prevailing wall-to-ambient temperature. The equation correlated from the heat loss experiments with different channel length-to-gap ratios, which calculate the heat loss flux using the measured local wall-to-ambient temperature difference, was incorporated into the data processing program to determine the local heat flux convected by the flow, q. The local Nusselt number, *Nu*, was subsequently determined using Eq. (1) with the thermal conductivity of coolant evaluated from the reference fluid temperature, T_f.

With each *Re*-L/B test option, five heater powers were adjusted to raise the central wall temperatures to the levels of 45, 75, 90, 120 and 145 °C. This attempt was aimed at varying the buoyancy level in order to explore the buoyancy effect on heat transfer. However, within the present parametric ranges tested, the variations of buoyancy level could only produce the maximum heat transfer variations of about ±4.2%. Therefore, the influences of buoyancy interaction on heat transfer in the present study were considered as insignificant. No further data analysis was followed to examine the buoyancy effect on heat transfer.

The experimental repeatability of temperature measurement using NEC TH3101-MR infrared radiometer was carried out prior to the baseline experiments. The maximum variations of wall temperature measurements with the flows to reach the same steady state conditions were in the range of ±0.7 °C. Thus the maximum uncertainty of temperature measurement was estimated as ±0.7 °C, which became the major source to attribute the uncertainties for the coolant's thermal conductivity, fluid density and viscosity. Following the policy of ASME on reporting the uncertainties in experimental measurements and results [20], the maximum uncertainty associated with the local Nusselt and Reynolds numbers were estimated to be 12.3 and 6.9% respectively.

3. Results and discussion

3.1. Baseline results

The baseline results obtained from the smooth-walled fin surface with heat transfer physics in channels with side open-boundaries and bottom sealed-end is compared with the data generated from those with rib-roughened fin surfaces. Fig. 3 shows the distribution of Nusselt number contours over the flat-fin surfaces of channels with L/B ratios of 5.89, 13.56 and 21.33 obtained at Reynolds numbers of 3000. As demonstrated in Fig. 3(a), the typical patterns of

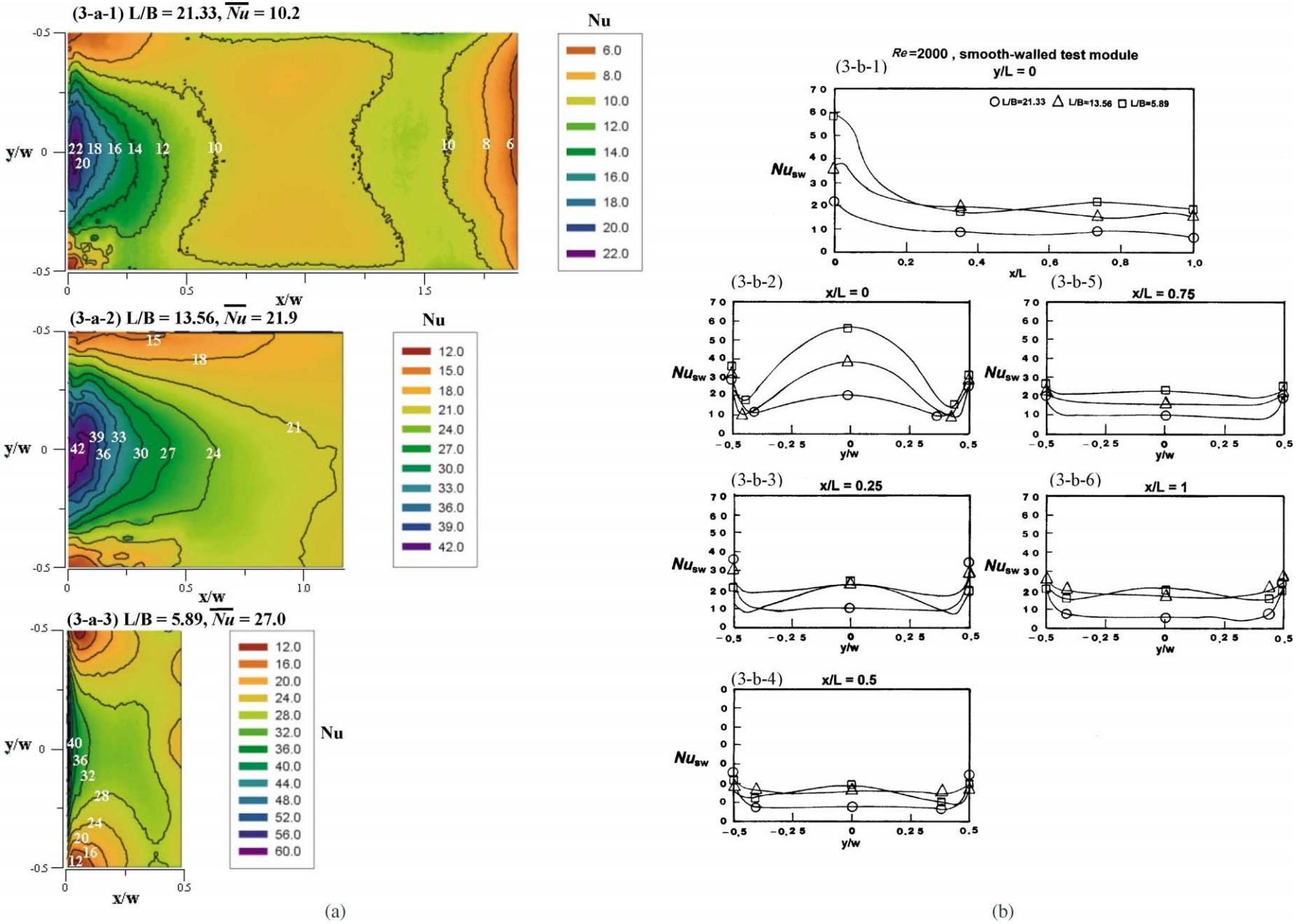

Fig. 3. Heat transfer results over smooth-walled fin surfaces. (a) Spatial distributions of Nusselt number contours over smooth-walled fins at Reynolds number of 3000. (b) Streamwise and spanwise Nusselt number distributions over smooth-walled fins at Reynolds number of 2000.

spatial heat transfer distribution, which show considerable dependency on the L/B ratio of test channel, reveal the characteristic heat transfer results for finned flow. In this regard, the distributions of Nusselt number contours are symmetrical about the streamwise centerline. The development of high convective capability in the central region of immediate flow entrance along with the streamwise decayed Nusselt number levels toward the bottom sealed end are also clearly observed. These general heat transfer features for fin-flows reflect the impact of side-profile leakage flows which clearly exhibit the impeding influences on downstream heat transfers as a result of undermined streamwise coolant mass flux, especially in the long fin channel. Therefore, the region with worse heat transfer scenarios accompanied by moderate spatial heat transfer variations occupies the majority of areas in the long fin channel ($L/B = 21.33$). The spatially averaged heat transfer over each fin surface, as indicated in each plot of Fig. 3(a), thus increases with the decreased L/B ratio. Unlike the well-confined ducted flows, there are two weak convective flow regimes developed at two upper corners of each fin surface as revealed in Fig. 3(a). These two upper-corner impeding heat transfer regions are clearly distinguishable in the streamwise region of $x/W < 0.25$ over the short fin surface ($L/B = 5.89$) where the most considerable impeding impacts of side-profile leakage flows on local heat transfers develop. As the side-profile leakage flow could gain a large momentum from the main coolant stream at the immediate flow entrance, the relatively large amount of coolant mass flux was lost into the ambient from two upper corners of the side openings. Accordingly, considerable local heat transfer impediment was generated. In this respect, the degree of heat transfer impediment developed at two upper corners of the opened fin channel decreased with the increased L/B ratio at fixed Reynolds number. A review of all the heat transfer images generated from flat-fin surfaces confirms that these upper-corner impeded heat transfer regions gradually expand toward the interior of the fin surface, either by reducing the L/B ratio at fixed Reynolds number or by increasing Reynolds number at fixed L/B ratio. Also revealed in Fig. 3(a) is a narrow bandwidth with relatively high heat transfer rates developed along two outer edges of side profiles on each fin surface. This local heat transfer enhancement along the open boundaries is related with the locally improved fluid mixing between ambient and hot leaking plenum. This effect is dependent on streamwise location and is clearly shown in Fig. 3(b).

The heat transfer variations along the streamwise centerline and across the flat-fin surfaces at five different streamwise locations for test channels with L/B ratios of 5.89, 13.56 and 21.33 at Reynolds number of 2000 are compared in Fig. 3(b). Note that, in Fig. 3(b), the streamwise coordinate, x, is alternatively normalized by each length of test channel, L, in order to compare the heat transfer results acquired from three test channels with different lengths. In view of the spanwise heat transfer variations obtained with L/B ratios of 5.89, 13.56 and 21.33 at different selective x/L locations, the heat transfer distributions are symmetrical about the streamwise centerline with various distribution patterns found at different x/L locations. As the spanwise heat transfer variation for all three test-channels is sensitive to the streamwise location, the forced convective fin-flow is three dimensional in nature. At the location of $x/L = 0$, the local heat transfer peak-values develop at the central location ($y/w = 0$). Further extending the spanwise coordinate toward two side edges causes the continuously monotonic heat transfer reductions up to the location of about ± 0.4 y/w at which the heat transfers to be increased. As illustrated previously, the local heat transfer increments over the narrow near-edge bandwidth are attributed to the enhanced local fluid mixing between the side leakage flow and the cold ambient. These phenomena persist almost over the entire length of each test channel. However, such spanwise bell-shape heat transfer variations could only persist onto 0.5 and 0.25 x/L for channels with L/B ratios of 5.89 and 13.56 or 21.33 respectively. Further downstream beyond these streamwise locations, where the spanwise bell-shape-like heat transfer variations develop, the spanwise variations of Nusselt numbers in the core regions of flat-fin surfaces distribute uniformly. For the case of $Re = 500$ and $L/B = 21.33$, the Nusselt numbers along the spanwise axis (Y axis) at the location of 1 x/L almost approach zero values. This physically reveals the vanished forced convective capability due to the development of a stagnant-like plume over the bottom sealed-end as an effect of accumulative side-profile leakages. Fig. 3(b) also reveals that the distributions of local Nusselt numbers along the streamwise centerline gradually decrease from the flow entrance level toward the low heat transfer region at the bottom sealed-end with the detailed distribution patterns affected by L/B ratio. This continuous streamwise decay in local heat transfer revealed in Fig. 3(b) reflects the influences of side-profile leakages on heat transfer, which has modified the nature of constant heat transfer rate in the developed flow region of ducted flow. A review of all versions of Fig. 3(b) for all the Reynolds numbers tested, which cover the laminar, transitional and turbulent flow regimes, ensures that the local heat transfer levels are consistently elevated by either increasing Reynolds number or shifting the flow regimes upstream towards the flow entrance for all three tested channels.

3.2. Rib-roughened channels

The heat transfer augmentation over a fin surface was attempted by fitting the repeated transverse ribs on two opposite walls of the opened fin-channel in a staggered manner. The heat transfer physics revealed from the baseline study have demonstrated that the side leakages of coolant flow could considerably affect the spatial distributions of coolant mass flux. This consequently modifies the heat transfer from the ducted-flow scenarios. The typical rib effects found in the ducted flows [16–19] are subject to modifications for fan-fin flow configuration. It is with the combined effects of side-

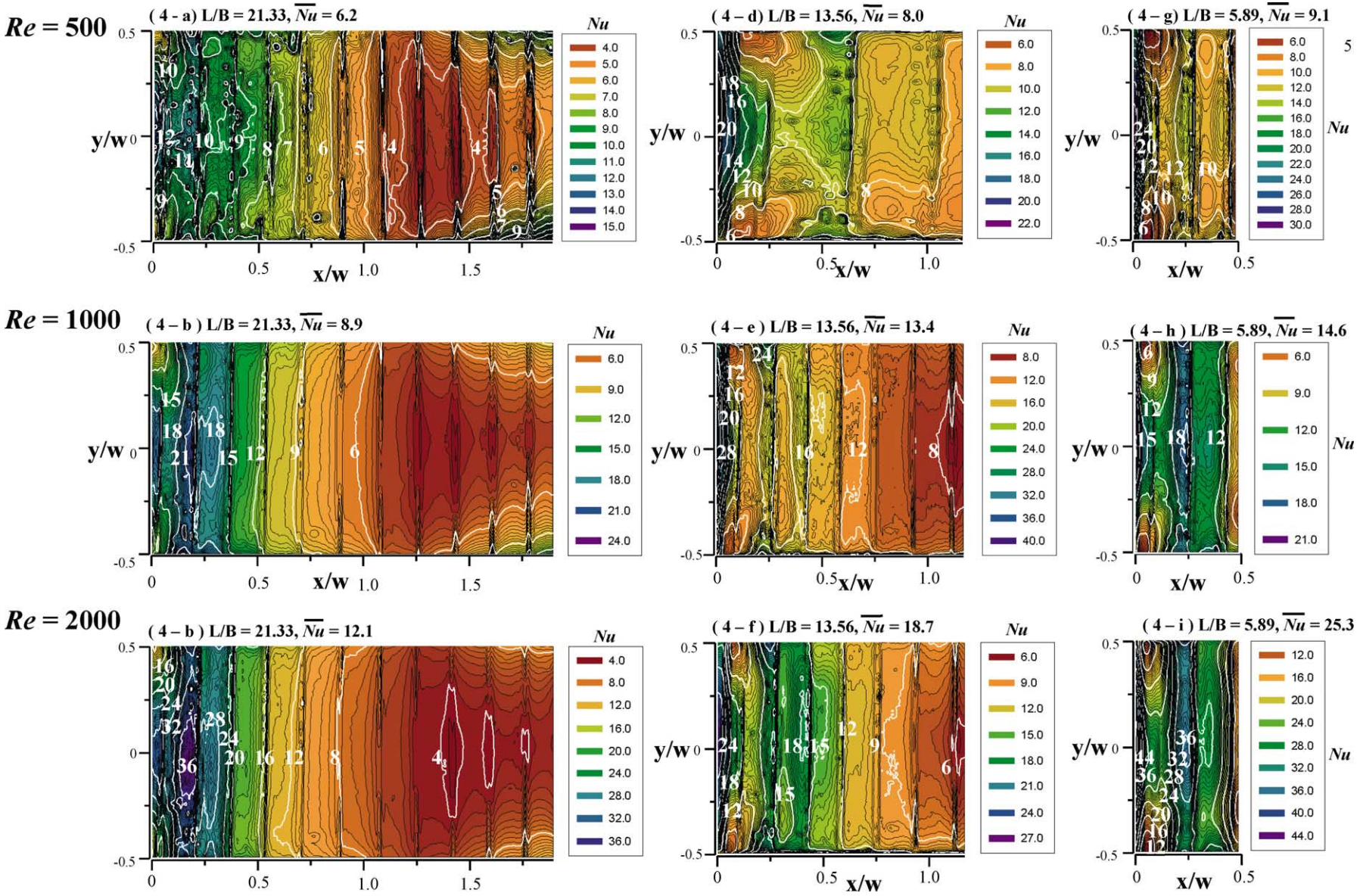

Fig. 4. Distributions of Nusselt number contours over rib-roughened fin surfaces at Reynolds numbers of 500, 1000 and 2000.

profile leakage flows with the rib-induced flow phenomena on heat transfer that the present section is addressed. Fig. 4 illustrates the distribution of Nusselt number contours over the rib-roughened fin surfaces in channels with L/B ratios of 5.89, 13.56 and 21.33 obtained at Reynolds numbers of 500, 1000 and 2000. The impact of varying Reynolds number and channel L/B ratio on the detailed heat transfer distributions are respectively examined by comparing the contour plots shown in each column and each raw of Fig. 4. The rib-roughened test channels share several characteristic heat transfer features revealed in the baseline study. These features include the spanwise symmetrical heat transfer distributions, the better cooling performance in the central region of immediate flow entrance, the streamwise weakened heat transfer toward the bottom sealed-end, and the development of upper-corner heat transfer impeding regions that still remains to typify the major impact of side-profile leakage flows on heat transfer. As shown in Fig. 4, the weakened downstream mass flux of coolant flow has led to poorer heat transfer scenarios with moderate spatial variations developed in the regions of $x/w > 0.75$, especially for the long fin channel. The spatially averaged heat transfer, as indicated in each plot of Fig. 4, generally increases with the decreased L/B ratio or with he increased Reynolds number. Although the two upper-corner weak convection zones also develop on the rib-roughened fin surface, these two heat-transfer impeding regions are considerably diminished. There is less sensitivity on the L/B ratio and Reynolds number in comparison with the scenarios found in the smooth-walled fin channels. Implicitly demonstrated by such comparative difference in this regard is the weakened spanwise momentum of side-profile leaking flow near the upper corners of rib-roughened channel. This phenomenon has led to the development of relatively large amounts of heat transfer enhancement from the smooth-walled references provided by the transverse ribs in the flow entry region. This effect will be examined in more detail when the effectiveness of heat transfer augmentation generated by the present surface ribs is examined.

The locally improved heat transfer levels along two side edges of each test channel relative to the interior counterparts are also distinguishable over the rib-roughened fin surfaces. Thus, the locally improved fluid mixing between ambient and coolant stream stirred by the side-profile leakage flow along the side edges of each test channel could lead to local heat transfer improvement on both smooth-walled and rib-roughened fin surfaces. It is worth noting that the contour plots collected in Fig. 4 show the additional impact of rib-induced flow phenomena on heat transfer by which the locally high heat transfer levels with dense contour distributions consistently develop on the rib surface relative to its adjacent flat areas between each pair of ribs. Such local heat transfer differences between rib and mid-rib regions gradually become vague in the further downstream locations as the streamwise momentum of coolant flow is consistently weakened by the increase of accumulated side leakages of coolant.

The detailed comparisons of heat transfers in three rib-roughened channels with L/B ratios of 5.89, 13.56 and 21.33 are shown in Fig. 5. This is done by plotting the heat transfer variations along the streamwise centerline and across the channel width at five different streamwise locations with Reynolds number of 2000. The heat transfer performances developed at the rib and mid-rib locations are distinctively different. In addition, the streamwise location in terms of x/L ratio embodies the percentage of total amount of coolant leakage that is a dominant factor affecting heat transfer. Therefore, the spanwise heat transfer variations at approximately same x/L location are collected at either rib or mid-rib locations from three rib-roughened channels to perform such a comparison. In view of the heat transfer distributions along the streamwise centerline over three rib-roughened surfaces (see Fig. 5-a), the locally high Nusselt number values consistently develop at the rib locations relative to their downstream mid-rib regions. However, as shown in Fig. 5-a, the distinguishable rib-induced heat-transfer augmentations for all three rib-roughened test channels tend to be initiated from their second ribs. As the boundary layer developments over the three heated test channels have proceeded about $10d$ in the flow calming chamber prior to interacting with the opened fin surfaces, the vague rib effect on heat transfer observed at the first rib location for all three test channels are related with the considerable amount of side-profile leakages. The rib-induced spatially heat transfer oscillations are most marked in the flow entry region and gradually fade in the further downstream, accompanied by streamwise reductions in heat transfer rates. The considerable streamwise reductions in the oscillating amplitudes of heat transfer variation between rib and mid-rib locations demonstrated in Fig. 5-a again reflect the impact of continuous side leakages of coolant mass flux on heat transfer. The spatial Nusselt number oscillations in channels with L/B ratios of 13.56 and 21.33 are almost indistinguishable after flow traverses about four ribs as compared in Fig. 5-a. Nevertheless, after examining all the versions of Fig. 5-a over the entire range of Reynolds numbers tested, it is confirmed that the increase of Reynolds number could considerably intensify the degree of such spatial heat transfer oscillation.

In Fig. 5, it is worth noting that the rib-roughened channel with L/B ratio of 5.89 could no longer consistently provide the highest heat transfer rates among the three test channels in the flow entry region. When the different length of each test channel normalizes the x coordinate, the same x/L ratio indicated in Fig. 5 corresponds to three different x/w locations in channels with L/B ratios of 5.89, 13.56 and 21.33. The first rib locations in three test channels thus appear at different x/L locations (see the arrows in Fig. 5-a). As shown in Fig. 5-a, the test channels with L/B ratios of 13.56 and 21.33 consistently offer better cooling performances at their second rib locations relative to

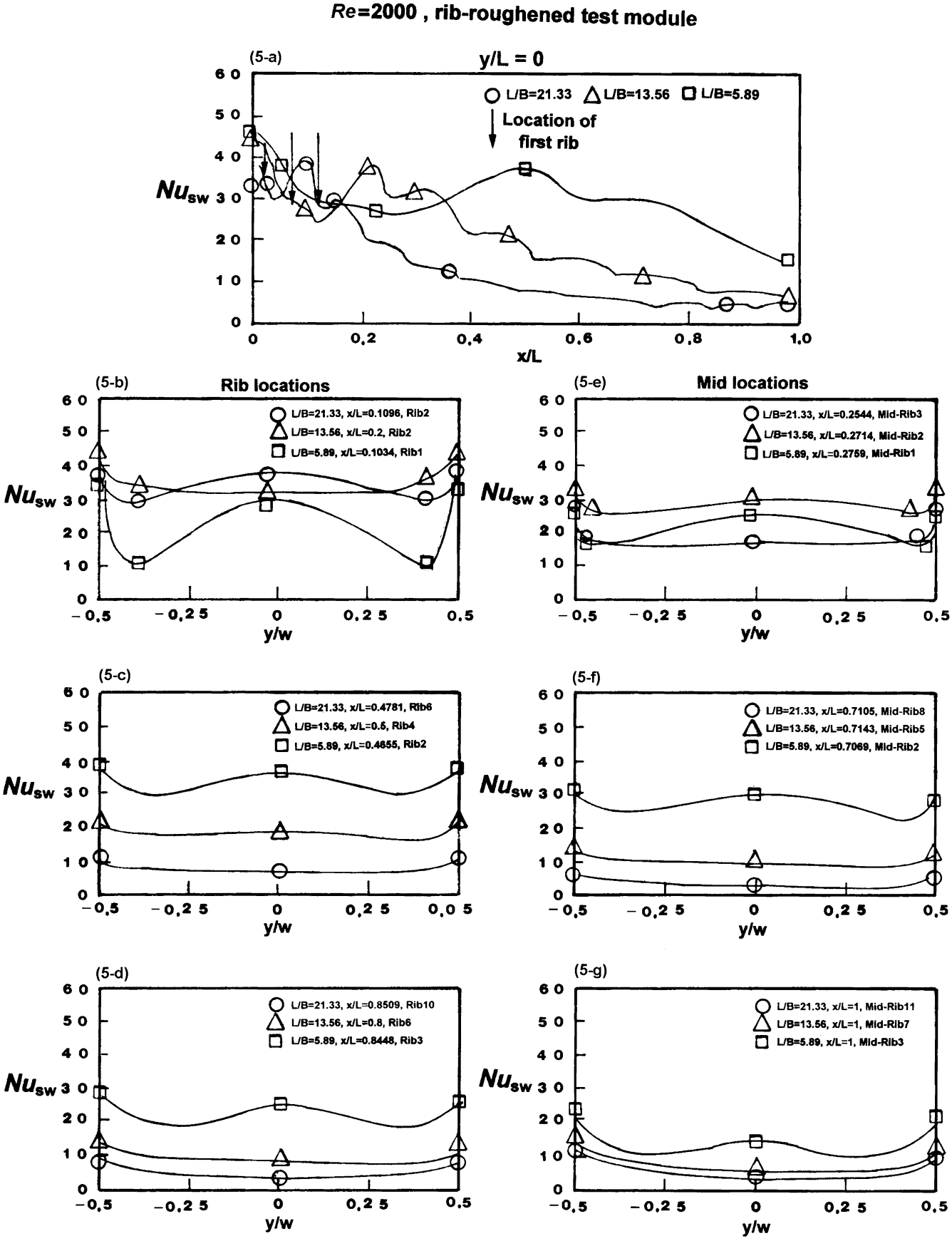

Fig. 5. Streamwise and spanwise heat transfer variations over rib-roughened fin surfaces at Reynolds numbers of 2000.

the counterparts at the same x/L locations. This particular comparative result is similarly observed with test results obtained at Reynolds numbers of 1000, 3000 and 3300. A close examination of this regard is shown in Fig. 5-b where the spanwise heat transfer variations detected at locations about $x/L = 0.1 \sim 0.2$ in three rib-roughened channels are compared. The channel with L/B ratio of 5.89 shows the lower Nusselt number values across the spanwise width in comparison with the counterparts in channels with L/B ratios of 13.56 and 21.33 (see Fig. 5-b). Note that the locations about 0.2 x/L correspond to the first rib location in the short channel ($L/B = 5.89$) and the second rib location in the middle-length channel ($L/B = 13.56$) and long channel ($L/B = 21.33$). As it has been demonstrated in Fig. 5-a that the distinguishable rib-induced heat-transfer augmentations for all three rib-roughened test channels initiate from their second ribs, the comparative difference between three test channels shown in Fig. 5-b is produced. In the x/L regions ($X/L > 0.5$) where the flow has traversed four ribs in the test channels with L/B ratios of 13.56 and 21.33, the rib-effects become very vague in these two channels (see Fig. 5-a).

It is clear that detailed streamwise heat transfer variations have been considerably modified from the smooth-walled references due to the presence of surface ribs. These repeated transverse ribs also affect the manners of spanwise heat transfer variations. As an illustrative example that compares the collective results obtained at Reynolds number of 2000 shown in Figs. 5 and 3-b, the degree of spanwise heat transfer variation in the rib-roughened channels are considerably moderated from the results detected in smooth-walled channels. The extension of spanwise coordinate toward two side edges of rib-roughened surface could still incur the continuously monotonic heat transfer reductions up to a spanwise location where the heat transfers deflect to be increased. However, this heat transfer behavior could only be prolonged to about the second rib location in the rib-roughened channels. These repeated transverse ribs interact with the side-leakage flows which require a considerable amount of coolant mass flux to facilitate the streamwise agitated flows and also the spanwise bell-shape-like heat transfer variations. Thus there is no apparent spanwise heat transfer variations generated at locations further downstream of the second rib where the streamwise agitating heat transfer variations start to be diminished. Consistent with the results found in the smooth-walled test channel, the spanwise distributions of Nusselt numbers rather flat in the further downstream locations where the spanwise bell-shape-like heat transfer variations diminish. Moreover, as surface ribs could be treated as the interior obstacles to weaken the downstream flow momentum, the hot plenum trapped over the bottom sealed surface could be more stagnant-like in the rib-roughened channels in comparison with the flow conditions developed in smooth-walled channels.

The streamwise and spanwise heat transfer variations depicted in Fig. 5 are typical for the test results obtained with $Re \geqslant 1000$. However, at the Reynolds number of 500, the version of Fig. 5 shows that the channel with L/B ratio of 5.89 could consistently provide the higher heat transfer rates than the channels with L/B ratios of 13.56 and 21.33. This agrees with the results found in the smooth-walled channels. Thus, the mechanisms identified from the baseline study could be the dominant physics for heat convection rather than the rib-associated phenomena when the inertial force of mainstream remains relatively weak ($Re = 500$). At the Reynolds number of 500, the heat transfers at the streamwise location of 1 x/L in all three rib-roughened channels are in close agreement. These have reduced considerably from the levels in flow entry regions due to the lack of flow momentum that incurs the development of stagnant-like hot plenum over the bottom sealed-end. There is therefore considerably suppressed the rib-induced heat transfer augmentation. It is worth emphasizing that, as the rib induced heat transfer enhancement is affected by the local streamwise momentum of flow, the impacts of side-profile leakage flows on the streamwise heat transfer reduction are amplified in the rib-roughened channel from the flat-fin scenarios. Relative to the conditions found in the smooth-walled channels, a larger degree of heat transfer improvement could be attained by either increasing Reynolds number or shifting the flow regimes upstream towards the flow entrance in the rib-roughened channels.

The heat-transfer augmentations provided by these surface ribs under the flow conditions developed in the opened fin channels are examined. The Nusselt number values detected from the rib-roughened fin surfaces, Nu, are normalized by the smooth-walled counterparts, Nu_{SW}. These ratios indicate the effectiveness of surface ribs on heat transfer augmentation. Fig. 6 shows the spatial distributions of Nusselt number ratio, Nu/Nu_{SW}, over the rib-roughened fin surfaces at Reynolds numbers 500, 1000 and 3000. As depicted in Fig. 6, the most considerable heat transfer augmentations generally develop in the flow entry regions. This observation agrees with the comparative result illustrated in Fig. 4 that the spanwise momentum of side-profile leakage flow near the upper corners of rib-roughened channel is weakened from the condition incurred in the likewise smooth-walled channel. In the channels of L/B ratios of 13.56 and 21.33, the Nusselt number ratios, Nu/Nu_{SW}, shown in Fig. 6, gradually reduce from unity to the values about 0.8 when the flow transverses about four pairs of ribs. However, in the short channel ($L/B = 5.89$), the effective region where the considerable heat transfer augmentations develop could only proceed onto the second rib location. Beyond this region the Nusselt number ratios, Nu/Nu_{SW}, could be reduced to levels of less than unity. The locally impeding heat-transfer effects in the further downstream due to these surface ribs are demonstrated as a result of considerably weakened streamwise momentum. With the lesser amount of flow momentum to agitate the enhancement of vorticity and/or turbulence intensity, these surface ribs in the impeding heat trans-

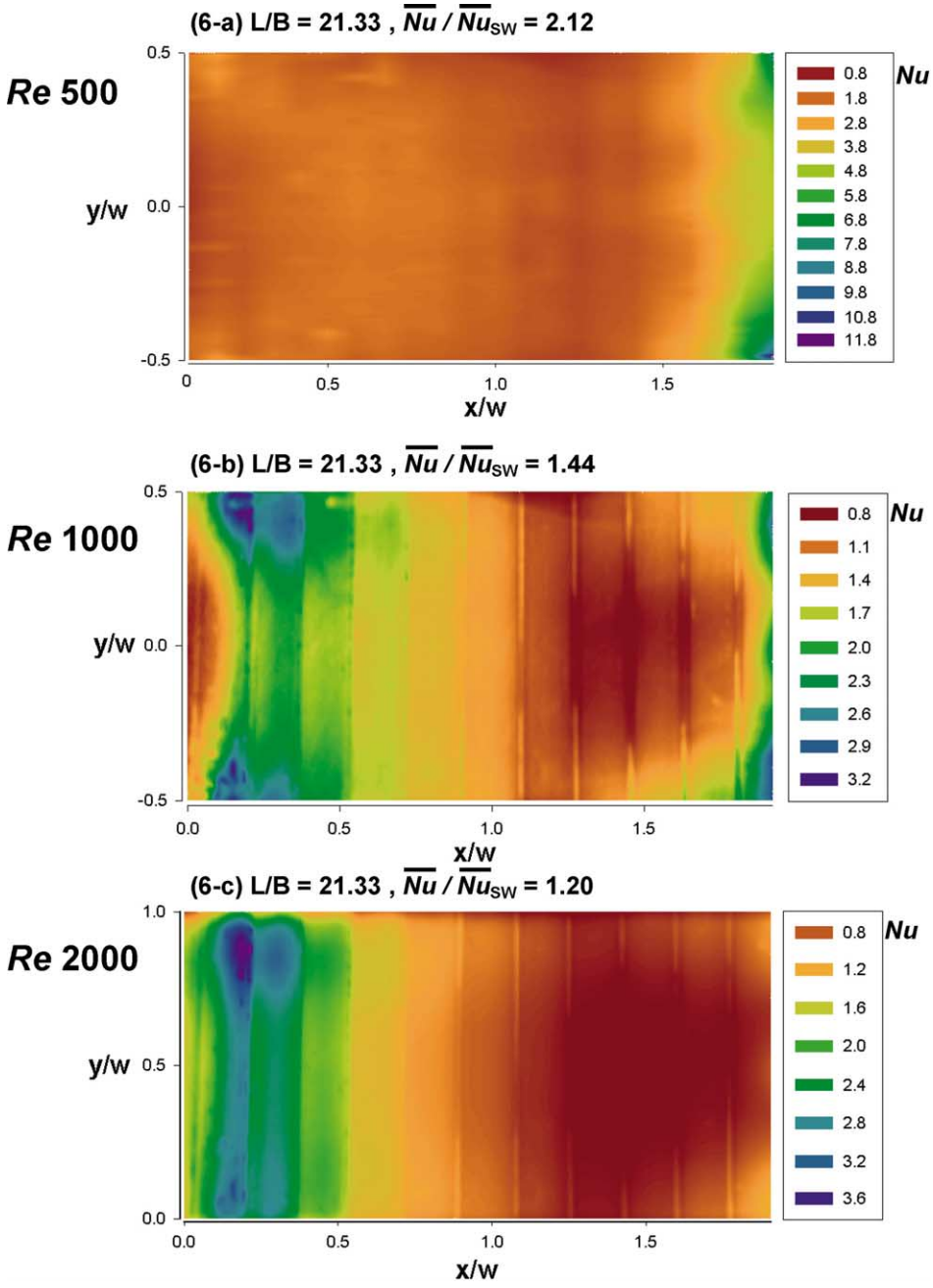

Fig. 6. Distributions of Nusselt number ratio, Nu/Nu_{sw}, over rib-roughened surfaces.

fer regions are alternately treated as the repeated obstacles to weaken the streamwise flow momentum. This particular heat transfer phenomenon could provide a profound influence on determining the optimal L/B ratio for the rib-roughened fin channel. As an overall indication of the effectiveness of the present surface ribs on heat transfer augmentation, the review of the entire sets of data processed is illustrated in Fig. 6. This shows that the augmentation of spatially averaged heat transfers provided by the present surface ribs are in the range of 140–200% of the smooth-walled channel levels.

3.3. Heat transfer correlation

The heat transfer results typified in Figs. 4 and 5 mainly reflect the impact of surface ribs and side-profile leakage flows on local heat transfers. This is for conditions with various L/B ratios and Reynolds numbers through mechanisms which involve the interaction of mainstream mass flux with side-profile leakage flow, local fluid mixing of side leakage with cold ambient along the open boundaries, and associated rib flow phenomena. As these mechanisms are interrelated with L/B ratio and *Re*, the inter-correlation caused by the coupling L/B-*Re* effects are expected prior to de-

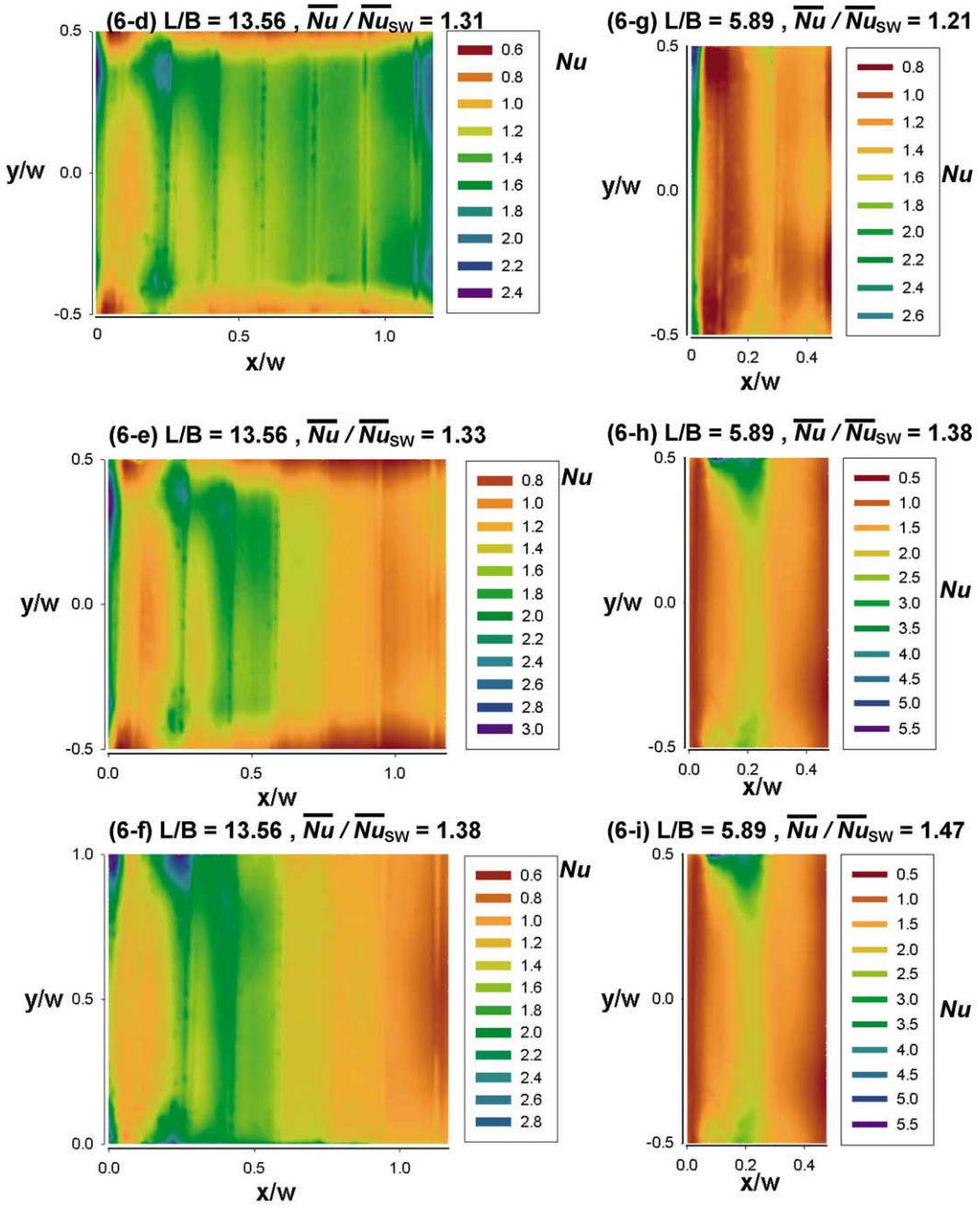

Fig. 6. Continued.

riving the heat transfer correlation. For engineering applications, it is essential to evaluate the convective capabilities over each rib-roughened fin surface with various flow conditions in order to determine the cooling duty of a fan-fin assembly. Therefore the local Nusselt numbers over each rib-roughened fin surface generated with all the Re-L/B options are spatially averaged to acquire the spatially averaged Nusselt number data, $\overline{Nu}$, for further data analysis aimed at disclosing its regressive-type equation. In the quest to identify the L/B ratio effect on the spatially averaged heat transfer; three sets of data generated from test channels with L/B ratios of 5.89, 13.56 and 21.33 are compared in Fig. 7. This is done to illustrate the variations of spatially averaged Nusselt number, $\overline{Nu}$, with the Reynolds number. It is clearly demonstrated in Fig. 7 that the spatially averaged Nusselt number, $\overline{Nu}$, steadily increases with the increase of Reynolds number for all the channels tested. An asymptotic constraint of zero-forced convective capability when Re approaches zero indicates a boundary condition for the equation applied to correlate the data trends revealed in Fig. 7. Justified by all the versions of data trends revealed in Fig. 7 and considering the physical constraints when Re approaches zero, the

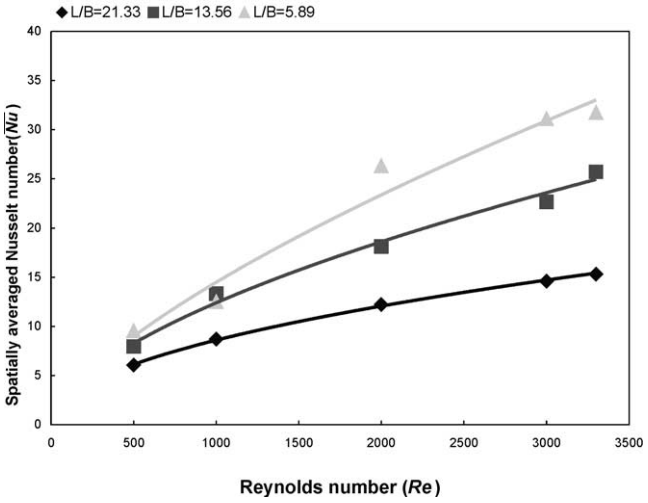

Fig. 7. Variations of spatially averaged Nusselt number with Reynolds number.

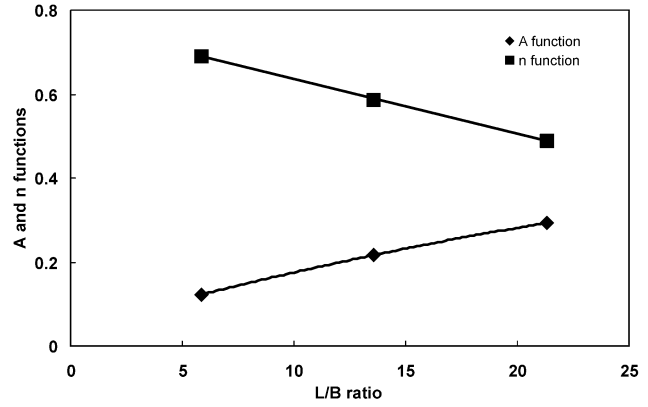

Fig. 8. Variations of A and n functions with L/B ratio.

data trends shown in Fig. 7 are correlated by the equation of

$$\overline{Nu} = A\left\{\frac{L}{B}\right\} \times Re^{n\{\frac{L}{B}\}} \tag{2}$$

where the A and n functions are the numerically determined curve-fitting coefficients. Because the overall convective capability over each fin surface involves the mutually interactive Re and L/B effects, the coefficient A and n are expected to be functions of the L/B ratio. Fig. 8 plots the variations of A and n functions when the L/B ratio increases for rib-roughened test channels. As depicted in Fig. 8, A and n functional values respectively follow the monotonically increasing and decreasing tendencies with an increased L/B ratio. The solid line that connects each data trend revealed in Fig. 8 is the fitted curve, using quadratic function with L/B ratio as the dependent variable. The net result of the data analysis is an empirical heat transfer Eq. (3) that evaluates the spatially averaged Nusselt number, $\overline{Nu}$, over the rib-roughened fin surface for a given set of L/B and Re values in the ranges of 5.89–21.33 and 500–3300, respectively.

$$\overline{Nu}\big|_{\text{rib-roughened surface}} = \left[0.0392 + 0.0151 \times \frac{L}{B} - 0.00015 \times \left(\frac{L}{B}\right)^2\right] \times Re^{0.7765-0.01507\times(\frac{L}{B})-7.491\text{E}-5\times(\frac{L}{B})^2} \tag{3}$$

The variations of coefficients A and n could be, respectively, treated as an indication of the interactive influences of rib-induced flow and side leakages and the convective inertial force effects on heat transfer. It is interesting to note that the correlated value of n exponent decreases from 0.7765 when the L/B ratio increases. The limiting value of n exponent (0.7765) at zero L/B ratio found in Eq. (3) is in close agreement with the well-established 0.8 value derived as the exponent of Reynolds number in the Nusselt number correlation for fully developed smooth-walled ducted flows [21]. The physical implication in this regard is that the asymptotic solution of Eq. (3) at $L/B = 0$ reflects the heat transfer performance at the immediate exit of the flow calming section. This, in turn, typifies the scenarios of ducted flow with rectangular sectioned shape. When the L/B ratio increases, the exponent n decreases correspondingly. This result physically indicates the weakened forced convective inertial effects on heat transfer due to the increased side-profile leakages. Corresponding with the decreasing trend of exponent n, the A functional values increase with the increased L/B ratio. It is revealed in Fig. 8 that the correlating curve of the quadratic function with an L/B ratio as the dependent variable provides satisfactory agreement at all data points. The net result generated in this phase of data analysis is an empirical correlation of Eq. (3). This permits the evaluation of influences of individual and compound L/B and Re effects on spatially averaged heat transfer over the fin surface roughened by repeated transverse ribs in a channel with side openings and bottom sealed end. The overall success of this correlation is indicated in Fig. 9, where all the experimental data are compared with the correlative prediction provided by Eq. (3). As revealed in Fig. 9, the spatially averaged Nusselt numbers fall in the range of 5–34.8 with three distinguishable data clusters generated by different L/B ratios. The max-

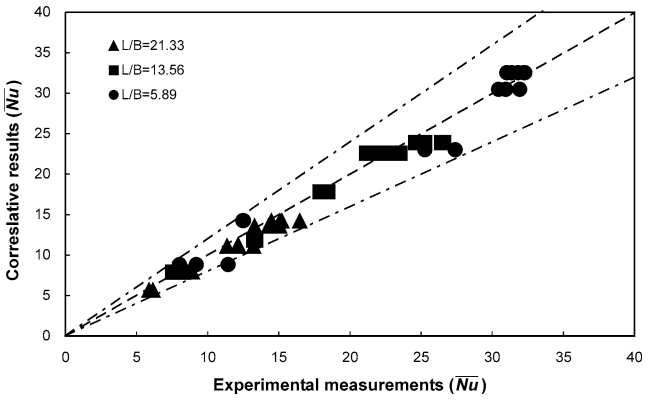

Fig. 9. Comparison of correlation predictions of spatially averaged Nusselt number with experimental results.

imum discrepancy of ±20% between the experimental and correlating results is achieved for 98% of the entire data generated.

Although it has been revealed that the decrease of channel length-to-gap ratio could generally improve the spatially averaged heat transfer over the flat fin surface, the cooling area (fin surface) is also accordingly reduced. The optimal selection of an L/B ratio for an opened fin channel fitted with transverse ribs offers the maximum convective heat flux from the fin surface. Consideration of improved spatially averaged Nusselt numbers together with the reduced cooling area when the L/B ratio decreases are essential. Note, as the width-to-gap ratio of three test channels is fixed by the present study, the surface area of each finned channel is the function of L/B ratio. In the attempt to disclose the optimal value of the L/B ratio for a forced convective rib-roughened fin assembly that generates the maximum convective flux from a fin surface, each spatially averaged Nusselt number data, $\overline{Nu}$, is multiplied with the L/B ratio at a particular Reynolds number tested. As the present test configuration fixed the width-to-gap ratio of test channel, the combined dimensionless heat transfer data in terms of $\overline{Nu} \times \frac{L}{B}$ features the overall convective heat flux transferred by the coolant flow over the rib-roughened fin surface. The variation in overall heat convection capability in terms of $\overline{Nu} \times \frac{L}{B}$ with L/B ratio at each predefined Reynolds number examined are illustrated in Fig. 10. Note that the asymptotic scenarios for zero fin length ($L = 0$) are reduced to the heat transfer solutions of impinging slot jets onto flat surface with finite values of convection coefficient in terms of $\overline{Nu}$. However, there is no fin effect in this case so that the value of $\overline{Nu} \times \frac{L}{B}$ has to be zero when the fin-length diminishes to zero. As depicted in Fig. 10 for each *Re* controlled curve, the peak value of $\overline{Nu} \times \frac{L}{B}$ locates at a specific L/B ratio, which is defined as the optimal L/B ratio. It is clearly shown in Fig. 10 that the optimal L/B ratio varies with Reynolds number. Nevertheless, justified by the data trends and the physical constraint of vanished $\overline{Nu} \times \frac{L}{B}$ value when L/B ratio approaches zero, the data points shown in Fig. 10 are correlated into the general form of

$$\overline{Nu} \times \frac{L}{B} = C\{Re\} \times \frac{L}{B} + D\{Re\} \times \left(\frac{L}{B}\right)^2 \tag{4}$$

where C and D are the correlating coefficients for each data trend typified in Fig. 10 that vary with Reynolds number. The optimal value of L/B ratio that provides the maximum level of $\overline{Nu} \times \frac{L}{B}$ could be obtained based on the usual optimization concept, as follows:

$$\frac{\partial(\overline{Nu} \times \frac{L}{B})}{\partial(\frac{L}{B})} = 0 \quad \Rightarrow \quad \left.\frac{L}{B}\right|_{\text{Optimal value}} = -\frac{C\{Re\}}{2D\{Re\}} \tag{5}$$

As the correlating coefficients C and D are functions of Reynolds number, the optimal L/B ratio that permits the maximum convective heat flux transferred by coolant flow for a rib-roughened fin assembly is Reynolds number dependent. Fig. 11 reveals the dependency of optimal L/B ratio on Reynolds number for the rib-roughened fin surface. A moderate decrease of optimal L/B ratio with increased Reynolds number is demonstrated in Fig. 11. Based on the results demonstrated in Fig. 11, the criterion for selecting the optimal L/B ratio of the open-boundary fin channel with fin surfaces roughened by transverse ribs is formulated as

$$\left.\frac{L}{B}\right|_{\text{Optimal value}} = 17.26 + 12.13 \times e^{-0.001373 \times Re} \tag{6}$$

In the *Re* range of 500–3300, Eq. (6) could be adopted as a design reference to define the length-to-gap ratio of a fin sink for the cooling device of an electronic chipset with intensified integration of electrical circuits.

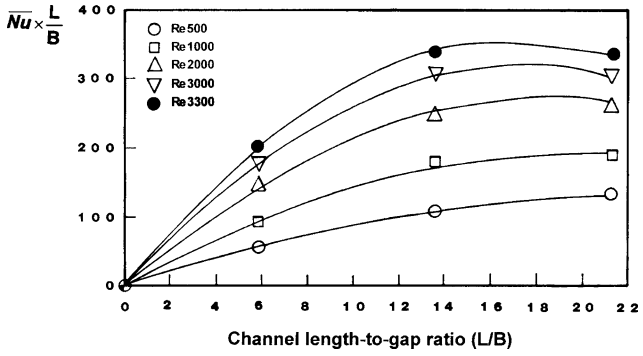

Fig. 10. Variations of $\overline{Nu} \times \frac{L}{B}$ with L/B ratio at fixed Reynolds numbers.

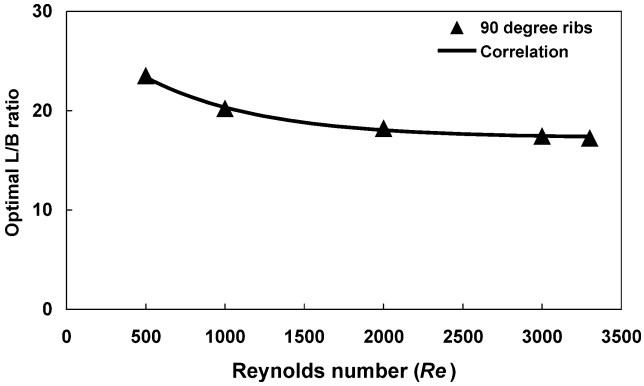

Fig. 11. Variation of optimal L/B ratio with Reynolds number for rib-roughened channel.

4. Conclusions

The detailed heat transfer measurements over three fin surfaces roughened by repeated transverse ribs on two opposite walls in channels with length-to-gap ratios of 5.89, 13.56 and 21.33, which are opened on the two side-profiles and sealed at the bottom-end, have been determined at Reynolds numbers of 500, 1000, 2000, 3000 and 3300. This attempted to generate the heat transfer correlations and to devise a design criterion for selecting the optimal length-to-gap ratio of a fin sink for cooling device of electronic packaging. The Reynolds number and channel height-to-gap ratio have demonstrated their impact on the local and spatially aver-

aged heat transfers. These were due to their interacting influences on the rib-induced flow phenomena and the side-profile leakage flows that consequently affect the spatial distributions of coolant mass flux and the effectiveness of surface ribs on heat transfer augmentation. These mechanisms, in association with L/B and *Re* variables, are inter-related which have led to the presence of coupling L/B-*Re* effects on the spatially averaged heat transfer. In conformity with the experimental evidence, the regression-type analysis was undertaken to generate the empirical heat transfer correlation that accounts for the spatially averaged Nusselt number over the rib-roughened fin surface. In addition was the wish to formulate a criterion for selecting the optimal L/B ratio that acquires the maximum convective heat flux from the rib-roughened fin surface. Several salient points that have been identified which may be summarized as follows.

(1) The characteristic heat transfer results from the rib-roughened fin-type channels involve the developments of streamwisely agitated heat transfer variations and high convective heat transfer capability in the central region of flow entrance. In addition, there is also a streamwise weakened heat convection toward the bottom sealed end, a narrow bandwidth with relatively high heat transfer rates along the side-profile openings, and local heat transfer impediments developed at two upper corners. These are due to interacting impacts of side leakage flows on the spatial distributions of coolant mass flux.

(2) The additional impact of rib-induced flow phenomena generates the locally high heat transfer levels with dense contour distributions over the rib surface relative to its successive mid-rib surfaces. The distinguishable rib-induced agitated streamwise heat transfer variations tend to be initiated from the second rib location and diminished at the fourth rib in the present range of Reynolds numbers tested. The augmentation of spatially averaged heat transfers generated by the present surface ribs is in the range of 140–200% of the smooth-walled channel levels.

(3) The proposed $\overline{Nu}$ correlation is consistent with the experimentally revealed heat transfer physics that permitted the individual and interactive effects of *Re* and L/B ratio on spatially averaged heat transfer over a rib-roughened fin surface to be evaluated.

(4) A criterion for selecting the optimal L/B ratio that provides the maximum convective heat flux from the rib-roughened fin surface has been devised for design applications. This which reveals that he optimal L/B ratio decreases with *Re* in the rib-roughened channels for fan-fin type flows.

Acknowledgements

This work was financially supported by the National Science Council, Taiwan, R.O.C. under the grant number of NSC 90-2611-E-022-001 to the National Kaohsiung Institute of Marine Technology. The efforts devoted by two of our research students, namely Wang, Po Sen and Huang, Chih Chung, toward the data collection and analysis are gratefully acknowledged.

References

[1] Intel corporation, Datasheet on Intel Pentium 4 processor with 512-KB L2 Cache on 0.13 micron process at 2 GHz, 2.2 GHz, 2.26 GHz, 2.4 GHz, 2.5 GHz, 2.53 GHz, 2.6 GHz, 2.66 GHz and 2.8 GHz, Document number: 298643-004, August (2002) 63.
[2] R.W. Knight, D.J. Goodling, J.S. Hall, R.C. Jaeger, Heat sink optimization with application to microchannels, IEEE Transactions on Components, Hybrids, and Manufacturing Technology 15 (5) (1992) 832–842.
[3] L.M. Su, S.W. Chang, Detailed heat transfer measurements of impinging jet arrays issued from grooved surfaces, Internat. J. Thermal Sciences 41 (2002) 823–841.
[4] A. Tabatabai, A. Faghri, A new two-phase flow map and transition boundary accounting for surface tension effects in horizontal miniature and micro tubes, ASME J. Heat Transfer 123 (2001) 958–968.
[5] P. Dutta, A. Beskok, T.C. Warburton, Numerical simulation of mixed electroosmotic/pressure driven microflows, Numerical Heat Transfer (A) 41 (2002) 131–148.
[6] L.G. Hansen, B.W. Webb, Air jet impingement heat transfer from modified surfaces, Internat. J. Heat Mass Transfer 36 (1993) 989–997.
[7] A. Mertol, Optimization of extruded type external heat sink for multichip module, ASME J. Electronic Packaging 115 (1993) 440–444.
[8] K. Azar, C.D. Mandrone, Effect of pin-fin density of the thermal performance of unshrouded pin-fin heat sinks, ASME J. Electronic Packaging 116 (1994) 306–309.
[9] M. Morega, A. Bejan, Plate-fins with variable thickness and height for air-cooled electronic modules, Internat. J. Heat and Mass Transfer 37 (1994) 433–445.
[10] G. Ledezma, A.M. Morega, A. Gejan, Optimal spacing between pin fins with impinging flow, ASME J. Heat Transfer 118 (1996) 570–577.
[11] R.A. Wirtz, R. Sohal, H. Wang, Thermal performance of pin-fin fan-sink assemblies, ASME J. Electronic Packaging 119 (1997) 26–31.
[12] S.B. Sathe, K.M. Kelkar, K.C. Karki, C. Tai, C.R. Lamb, S.V. Patankar, Numerical prediction of flow and heat transfer in an impingement heat sink, ASME J. Electronic Packaging 119 (1997) 58–63.
[13] S. Sathe, B. Sammakia, A review of recent developments in some practical aspects of air-cooled electronic packages, ASME J. Heat Transfer 120 (1998) 830–839.
[14] L.A. Brignoni, S.V. Garimella, Experimental optimization of confined air jet impingement on a pin fin heat sink, IEEE Trans. Component Packaging Technology 22 (1999) 399–404.
[15] H. El-Sheikh, S.V. Garimella, Heat transfer from pin-fin sinks under multiple impinging jets, IEEE Trans. Component Packaging Technology 23 (2000) 113–120.
[16] J.C. Han, Y.M. Zhang, C.P. Lee, Augmented heat transfer in square channels with parallel, cross, and *V*-shaped angled ribs, ASME J. Heat Transfer 113 (1991) 590–596.
[17] M.E. Taslim, T. Li, D.M. Kercher, Experimental heat transfer and friction in channels roughened with angled, *V*-shaped, and discrete ribs on two opposite walls, ASME J. Turbomachinery 118 (1996) 20–28.
[18] T.M. Liou, J.J. Hwang, Turbulent heat transfer augmentation and friction in periodic fully developed channel flows, ASME J. Heat Transfer 114 (1992) 56–64.
[19] S. Mochizuki, A. Murata, M. Fukunga, Effect of rib arrangements on pressure drop and heat transfer in a rib-roughened channel with a sharp 180 deg turn, ASME J. Turbomachinery 119 (1997) 610–616.
[20] Editorial Board of ASME Journal of Heat Transfer, Journal of Heat Transfer Policy on reporting uncertainties in experimental measurements and results, ASME J. Heat Transfer 115 (1993) 5–6.
[21] F.W. Dittus, L.M.K. Boelter, Californian pubs, Engrg. 2 (1936) 443.